Available online at www.sciencedirect.com
ScienceDirect
Journal of Solid State Chemistry 180 (2007) 2851–2858
JOURNAL OF SOLID STATE CHEMISTRY
www.elsevier.com/locate/jssc

Anion vacancy ordering in $Sr_7Mn_4O_{15-x}$ phases

Michelle O'Malley, Michelle A. Lockett, Michael A. Hayward*

Department of Chemistry, Inorganic Chemistry Laboratory, University of Oxford, South Parks Road, Oxford, OX1 3QR, UK

Received 26 June 2007; received in revised form 8 August 2007; accepted 9 August 2007
Available online 28 August 2007

Abstract

The synthesis of phases of composition $Sr_7Mn_4O_{15-x}$ $0<x<3$ is reported via the topotactic manipulation of the anion lattice of $Sr_7Mn_4O_{15}$. In addition the reduced, cation substituted phases $BaSr_6Mn_4O_{13}$ and $Sr_6CaMn_4O_{13}$ are described. Structural characterisation using powder X-ray and neutron diffraction data reveals that in all phases anions are selectively removed from sites which link the MnO_6 octahedra in the structure in an apex-sharing manner. An explanation based on the total lattice energy of the anion deficient phases is presented to account for this unusual selectivity.

Keywords: Neutron diffraction; Manganese oxides; Topotactic reduction

1. Introduction

Since the observation of large magnetoresistive ratios in mixed valent Mn(III)/(IV) oxides there has been considerable interest in these phases [1–3]. Different strategies have been employed to induce and control the mixed valent state including cation substitution and more recently the introduction of anion vacancies in reductive processes [4,5]. It is reasonable to expect that controlling the manganese oxidation state via *A*-cation substitution in cubic perovskites, for example, could be generally considered to be a 'rigid band' type process. With the exception of small structural distortions induced by changes to the structural tolerance factor on cation substitution (an effect that is of course important in determining the subtle interplay between localized and delocalized electronic behaviour) no dramatic structural changes are induced and the electronic structure of the host material is conserved. The same is not generally true of doping via the introduction of anion vacancies.

The strong interactions between manganese centres and their surrounding oxide ligands means the removal of an oxide ion does not simply add electrons into existing empty electronic states. The *d*-states of manganese which lie at or close to the Fermi energy are significantly perturbed by changes to the local point symmetry on oxide deintercalation leading to significant changes in the local electronic structure around the anion vacancy. Furthermore, anion vacancies generally have a larger tendency to order within structures than substituted cations. Thus the introduction of anion vacancies perturbs not only the point symmetry at manganese sites but also the translational symmetry of the host crystal structure and thus the electronic structure of the host phase. Therefore if we wish to utilize the introduction of anion vacancies as a method of doping mixed valent Mn(III)/(IV) phases, and other complex oxides more generally, a detailed knowledge and appreciation of the anion vacancy distribution and ordering in complex oxides and the effects it has on the electronic behaviour of these phases is essential.

$Sr_7Mn_4O_{15}$ has a rather complex structure [6]. The manganese oxygen lattice can be thought of as an array of Mn_2O_9 dimers constructed from pairs of MnO_6 octahedra sharing faces (Fig. 1a). These Mn_2O_9 units then share corners to form a buckled two-dimensional array (Fig. 1b). Structurally this arrangement is similar to that of 4H-$BaMnO_3$ in which Mn_2O_9 dimers share corners to form a three-dimensional array (Fig. 1c) [7]. The major difference between the manganese–oxygen networks in the two structures is that the Mn_2O_9 units in 4H-$BaMnO_3$ share all six of the apical oxide ions where as the Mn_2O_9

*Corresponding author. Fax: +44 1865 272690.
E-mail address: michael.hayward@chem.ox.ac.uk (M.A. Hayward).

0022-4596/$ - see front matter © 2007 Elsevier Inc. All rights reserved.
doi:10.1016/j.jssc.2007.08.012

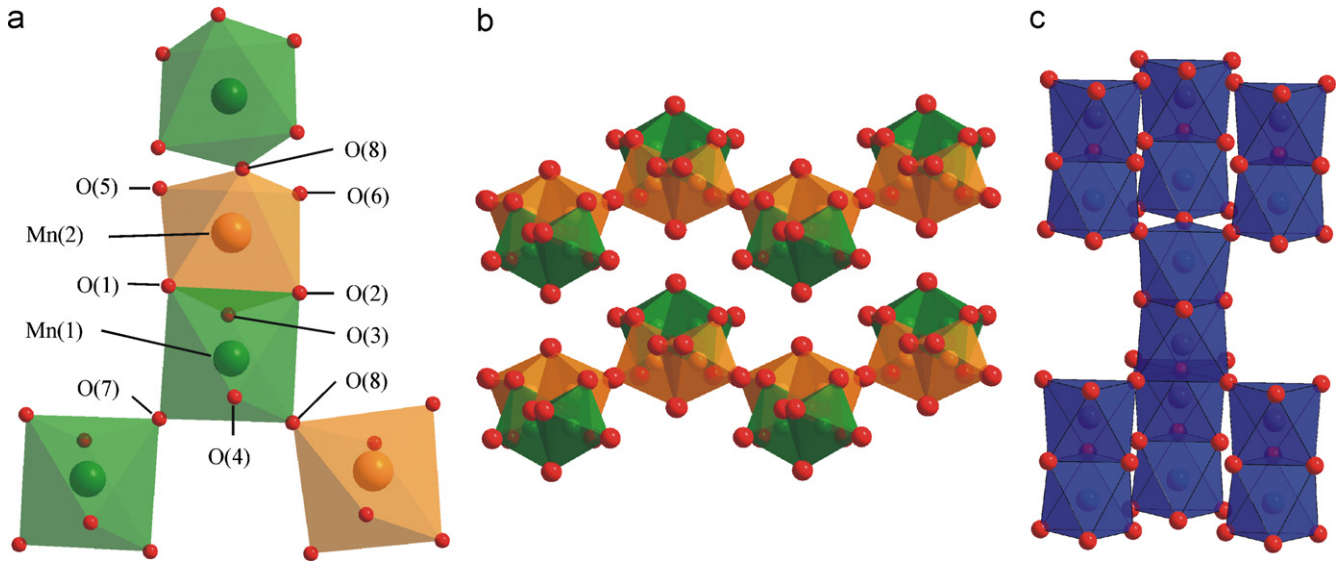

Fig. 1. The structure of $Sr_7Mn_4O_{15}$ showing (a) the manganese-oxygen connectivity and (b) the layered nature of the structure. (c) The manganese-oxygen connectivity in 4H-$BaMnO_3$.

units in $Sr_7Mn_4O_{15}$ are linked by only three of the six apical ions. The behaviour of these two phases on reduction however is significantly different. Reduction of $Sr_7Mn_4O_{15}$ to $Sr_7Mn_4O_{12}$ [8] removes oxide ions exclusively from the apex linked sites (O(7) and O(8) in Fig. 1a) whereas in the structure of 4H-$BaMnO_{2.66}$ the anion vacancies are located in anion sites which link the MnO_6 octahedra in a face-sharing manner [9]. Given the similarity of the manganese–oxygen networks in these two phases we set out to investigate this differing behaviour and if possible prepare compositions intermediate between $Sr_7Mn_4O_{15}$ and $Sr_7Mn_4O_{12}$.

2. Experimental

5 g samples of $Sr_7Mn_4O_{15}$, $BaSr_6Mn_4O_{15}$ and $Sr_6CaMn_4O_{15}$ were prepared via a citrate precursor method. Suitable quantities of $SrCO_3$ (99.994%), $BaCO_3$ (99.996%), $CaCO_3$ (99.9995%) and MnO_2 (99.999%) were dissolved in a 100 ml of 1:1 6 M nitric acid and distilled water. 10 mole equivalents of citric acid and 5 ml of analar ethylene glycol were added and the solutions heated with constant stirring. The gels thus formed was subsequently ground into a fine powder, placed in alumina crucibles and heated at 1 °C min^{-1} to 1000 °C in air. The resulting black powders were then pressed into 13 mm pellets at 5 tonnes pressure and heated in air at 1350 °C for 2 × 2 days with regrinding between heating periods. X-ray powder diffraction data collected from samples could be indexed on the basis of monoclinic unit cells (space group $P2_1/c$) and gave lattice parameters as shown in Table 1 in good agreement with previously reported values for these phases [6,10].

CaH_2 has been used in as a solid-state reducing agent to bring about the topotactic reduction of complex transition metal oxides according to reaction Scheme 1 [11].

$$ABO_3 + CaH_2 \Rightarrow ABO_{3-x} + xCaO + xH_2. \quad (1)$$

Table 1
Refined lattice parameters of $A_7Mn_4O_{15}$ phases

Phase	a(Å)	b(Å)	c(Å)	β(°)
$Sr_7Mn_4O_{15}$	6.8124(2)	9.6152(4)	10.3744(4)	91.865(3)
$BaSr_6Mn_4O_{15}$	6.8496(2)	9.6951(4)Å	10.4116(4)	91.671(2)
$Sr_6CaMn_4O_{15}$	6.7607(2)	9.5856(3)	10.3302(4)	91.713(3)

In order to investigate the reactivity of CaH_2 with $Sr_7Mn_4O_{15}$ as a function of temperature, small scale (~200 mg) reactions were performed. 4:1 stoichiometric ratios of CaH_2:$Sr_7Mn_4O_{15}$ were thoroughly mixed in a glovebox containing argon (O_2 and H_2O < 1 ppm) and then sealed in evacuated Pyrex ampoules (volume ~20 cm^3). Samples were heated at the desired reaction temperature (see Table 2) for two periods of 2 days, with intermediate regrinding. Danger: due to the hazards associated with the production of hydrogen gas in a sealed container at elevated temperature, this method is inappropriate for the synthesis of larger samples.

Larger samples (>1 g) suitable for neutron diffraction measurements were prepared using a vented reaction apparatus. In a glovebox, well ground mixtures of the substrate oxide to be reduced and CaH_2 were placed in an alumina boat contained within a glass tube sealed by means of a spring loaded vent valve, such that when the pressure in the tube was approximately half an atmosphere above ambient pressure the valve opened releasing gas into a stream of clean argon, as shown in Fig. 2. Prior to reaction the external gas flow was purged with argon via a 3-way

Table 2
Reaction conditions and lattice parameters of the products of reaction between $Sr_7Mn_4O_{15}$ and CaH_2

Reaction temperature (°C)	a(Å)	b(Å)	c(Å)	β(°)	Composition
300	6.8869(6)	9.8017(9)	10.0957(9)	94.138(1)	$Sr_7Mn_4O_{13.01(3)}$
350	6.9003(2)	9.7471(3)	10.0606(3)	93.88(1)	$Sr_7Mn_4O_{12.61(4)}$
360	6.910(1)	9.705(2)	10.042(2)	93.69(1)	$Sr_7Mn_4O_{12.23(4)}$
380	6.937(1)	9.665(2)	10.032(2)	93.41(1)	$Sr_7Mn_4O_{12.02(3)}$

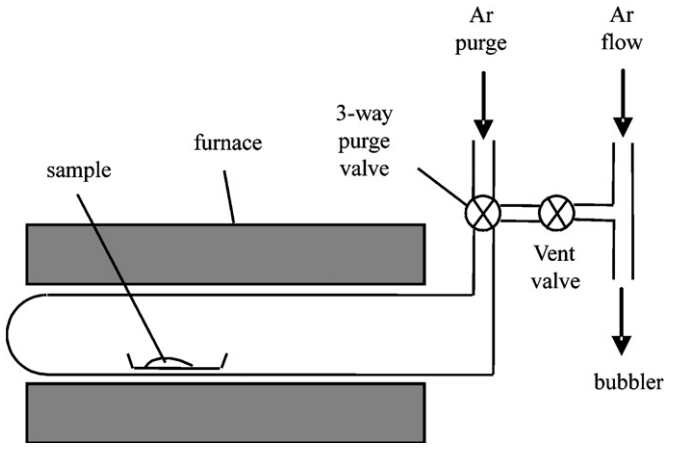

Fig. 2. Pressure venting apparatus used to reduce large samples with CaH_2.

valve. Utilizing this apparatus ~4 g samples were prepared by reacting a 4-fold stoichiometric ratio of CaH_2 with $A_7Mn_4O_{15}$ ($A_7 = Sr_7$, $BaSr_6$ or Sr_6Ca) at 300 °C for two periods of 2 days, with intermediate regrinding. Samples were then washed under nitrogen with 4×100 mL of a 0.25 M solution of NH_4Cl in methanol to remove the calcium containing phases (CaO, CaH_2). Samples were then washed with 4×80 mL of clean methanol to remove and remaining NH_4Cl, before being pumped to dryness.

The synthesis of phases of intermediate oxygen content was attempted via the comproportionation of $Sr_7Mn_4O_{15}$ and $Sr_7Mn_4O_{15-x}$ phases in a manner similar to the reported synthesis of $YSr_2Mn_2O_6$ [12]. Suitable quantities of the two phases were ground together, sealed in a Pyrex tube and heated to allow the oxygen content of the mixture to equilibrate.

In addition an alternative route to phases of intermediate oxidation state via controlled oxidation of $Sr_7Mn_4O_{15-x}$ phases was employed. On heating at 220 °C potassium permanganate decomposes according to reaction Scheme 2 [13].

$$2KMnO_4 \Rightarrow K_2MnO_4 + MnO_2 + O_2.$$

Thermogravimetric analysis of this reaction indicated that rather than the 2:1 molar ratio of $KMnO_4$:O_2 reported [13] the ratio was in fact 2:1.62 at the higher reaction temperatures to be employed (350 °C). Therefore 300 mg samples of $Sr_7Mn_4O_{15-x}$ were sealed in evacuated Pyrex tubes with suitable quantities of dried $KMnO_4$ contained within a separate glass liner such that the two manganese phases were not in physical contact. The reaction vessels were then heated at 350 °C to bring about the controlled oxidation of the $Sr_7Mn_4O_{15-x}$ samples.

Powder X-ray diffraction data were collected from samples contained within homemade air sensitive sample holders utilizing a Panalytical X'pert diffractometer incorporating an X'celerator position sensitive detector (monochromatic Cu$K\alpha$1 radiation). Neutron powder diffraction data were collected from samples contained within vanadium cans that had been sealed under argon with an indium washer. Data were collected using the HRPD instrument at the ISIS neutron source, Rutherford Appleton Laboratory, UK. Rietveld structural refinements performed against X-ray or neutron powder diffraction data utilized the GSAS suite of programs [14], specific details of the individual refinement procedures are noted in the text. Thermogravimetric data were collected from powder samples (~100 mg) using a Netzsch STA 409PC balance. Average manganese oxidation states in all phases were determined by dissolving samples in HCl containing an excess of KI and titrating the liberated I_2 with $Na_2S_2O_3$.

3. Results

Reactions between $Sr_7Mn_4O_{15}$ and CaH_2 evolve as a simple function of reaction temperature as shown in Table 2. Below 250 °C no reaction was observed. When the temperature was raised to 300 °C rapid reaction occurred yielding a phase of composition $Sr_7Mn_4O_{13}$, confirmed by thermogravimetric re-oxidation and iodometric titration. As the reaction temperature was raised further additional reduction occurred, ultimately yielding a phase of composition $Sr_7Mn_4O_{12}$ at 380 °C. The lattice parameters of this phase (Table 2) are consistent with previously reported values for $Sr_7Mn_4O_{12}$ prepared by the reduction of $Sr_7Mn_4O_{15}$ with sodium hydride [8]. Refinement of the structural model quoted for $Sr_7Mn_4O_{12}$ against high-resolution X-ray powder diffraction data collected from this sample yielded a good fit, further confirming the synthesis of $Sr_7Mn_4O_{12}$. Raising the reaction temperature above 400 °C led to rapid decomposition of the sample and the formation and SrO and MnO among other poorly crystalline products.

Despite numerous attempts it was not possible to prepare a phase of composition $Sr_7Mn_4O_{15-x}$ $0 < x < 2$ by reduction of $Sr_7Mn_4O_{15}$ with CaH_2. Attempts to prepare $Sr_7Mn_4O_{14}$ via the comproportionation of a 1:1 ratio

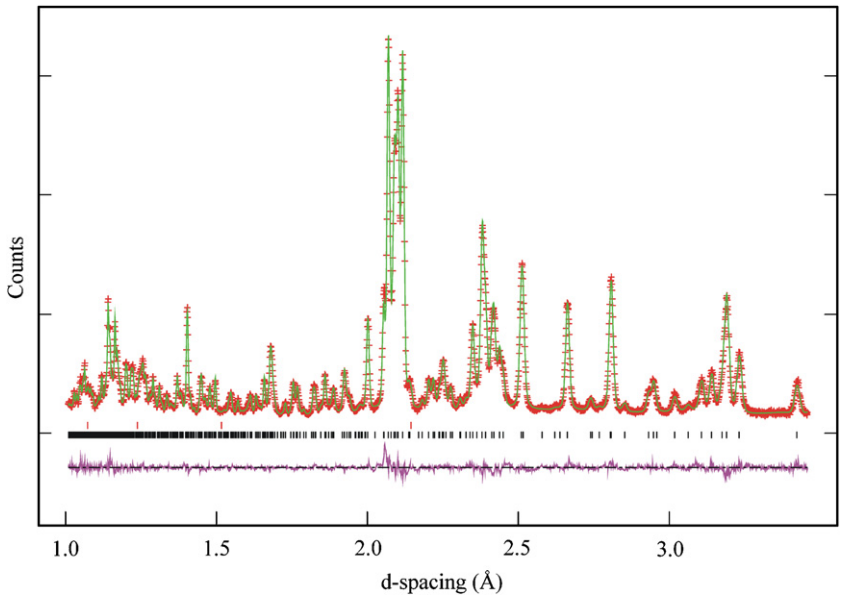

Fig. 3. Observed, calculated and difference plot from the structural refinement of $Sr_7Mn_4O_{13}$ against neutron powder diffraction data collected using the 90° detector bank of the HRPD diffractometer at ISIS. A second phase corresponding to elemental vanadium (upper tick marks) is included to account for contributions from the sample container.

$Sr_7Mn_4O_{15}$ and $Sr_7Mn_4O_{13}$ in a manner similar to the reported synthesis of $YSr_2Mn_2O_6$ [12], lead to the formation of the Ruddlesden–Popper phase Sr_2MnO_{4-x} [15] demonstrating the metastability of these reduced phases.

The controlled oxidation of $Sr_7Mn_4O_{13}$ with 0.308 mole equivalents of $KMnO_4$ at 350 °C yielded a sample of moderate crystallinity. Thermogravimetric reoxidation analysis and iodometric titrations indicated this sample had a composition of $Sr_7Mn_4O_{14.05(3)}$. Attempts to prepare large samples suitable for neutron diffraction analysis proved unsuccessful. The samples produced contained very inhomogeneous oxygen contents (multiple phases) and attempts to improve sample quality by annealing led to decomposition in line with the comproportionation reactions reported above.

X-ray and neutron powder diffraction data were collected from a sample of $Sr_7Mn_4O_{13}$ prepared as described above. These diffraction data could be readily indexed with a monoclinic unit cell and were consistent with $P2_1/c$ space group symmetry, suggesting this phase is structurally related to the 'parent phase' $Sr_7Mn_4O_{15}$. A model based of the structure of $Sr_7Mn_4O_{15}$ was therefore refined against the neutron diffraction data collected from this reduced phase. Initially a fully oxygen stoichiometric model was refined against the data resulting in a very poor fit. In order to locate the anion vacancies the occupation numbers of all the oxide ion sites were refined. The atomic displacement factors of all the anion sites were constrained to be the same to avoid any correlation effects during this process. After only a few cycles of refinement it became clear that one anion site (O(8)) had a very low occupancy, consistent with complete removal of this ion, while the remaining sites were fully occupied within error. The occupancy of the O(8) site was therefore set to zero and the remaining anion sites to unity while the atomic coordinates of all the atoms in the model were refined. Isotropic atomic displacement parameters were refined, but constrained by element or in the case of oxygen by structural type (face-sharing, corner sharing, non-bridging). In the final cycles of refinement the oxygen site occupancies were re-refined to confirm the anion vacancy distribution. The occupation numbers of all sites (with the obvious exception of O(8)) refined to values within 2% of full occupation and so were reset to unity. The occupancy of the O(8) site refined to a value of −0.02(2) and so was set to zero. The final refinement cycles readily converged with good agreement between observed and calculated diffraction patterns as

Table 3
Refined structural parameters for $Sr_7Mn_4O_{13}$

	x	y	z	Fraction	U_{iso}
Sr(1)	0.0100(3)	0.1810(2)	0.4634(2)	1	0.00157(6)
Sr(2)	0.3392(3)	0.1433(1)	0.1992(2)	1	0.00157(6)
Sr(3)	0.5	0	0.5	1	0.00157(6)
Sr(4)	0.1613(4)	0.0118(1)	0.8365(2)	1	0.00157(6)
Mn(1)	0.5739(5)	0.1640(4)	0.9210(4)	1	0.00105(7)
Mn(2)	0.7632(5)	0.1737(3)	0.7236(4)	1	0.00105(7)
O(1)	0.5051(3)	0.1062(2)	0.7280(2)	1	0.00140(6)
O(2)	0.6769(4)	0.1761(2)	0.3301(3)	1	0.00140(6)
O(3)	0.8420(4)	0.0899(2)	0.9150(2)	1	0.00140(6)
O(4)	0.3386(3)	0.2450(2)	0.9565(2)	1	0.00151(6)
O(5)	0.8407(3)	0.0267(2)	0.6235(2)	1	0.00151(6)
O(6)	0.0070(3)	0.2705(2)	0.7014(2)	1	0.00151(6)
O(7)	0.5	0	0	1	0.0028(1)

Space group: $P2_1/c$ $a = 6.8669(6)$ Å, $b = 9.8017(9)$ Å, $c = 10.0957(9)$ Å, $\beta = 94.138(1)°$, volume $= 677.7(2)$ Å^3 $\chi^2 = 2.12$, wRp = 4.23%, Rp = 4.48%.

shown in Fig. 3. Full details of the refined model are given in Table 3 with selected bond lengths in Table 6.

Similar procedures were employed to refine structural models against the data collected from $BaSr_6Mn_4O_{13}$ and $Sr_6CaMn_4O_{13}$. In these cases however, the *A*-cation occupancies was also refined to determine the Ba/Sr or Ca/Sr distribution in the samples. Full structural details given in Tables 4 and 5 and selected bond lengths in Table 6. Plots of fits to the experimental data can be found in the Supplementary information.

X-ray powder diffraction data collected from a sample of average composition $Sr_7Mn_4O_{14.05(3)}$ could be readily indexed on the basis of a monoclinic unit cell and were consistent with $P2_1/c$ symmetry. A model based on the structure of $Sr_7Mn_4O_{15}$ was refined against the data and a moderately good fit was achieved ($\chi^2 = 1.8$). Close inspection of the data revealed a number of asymmetric diffraction reflections suggesting a second phase was present in the sample. Given the slight oxygen excess in the sample, with respect to the target stoichiometry of $Sr_7Mn_4O_{14}$ a second phase corresponding to $Sr_7Mn_4O_{15}$ with lattice parameters fixed at those of the fully oxidized phase was added. This led to an improvement in the fit to the data ($\chi^2 = 1.36$) and accounted for the observed peak asymmetry. The lack of neutron diffraction data precluded the opportunity to study the structure of this phase in detail, particularly with reference to the location of the anion vacancies. Refined lattice parameters and phase

Table 4
Refined structural parameters for $Sr_6CaMn_4O_{13}$

	x	*y*	*z*	Fraction	U_{iso}
Sr/Ca(1)	0.0068(4)	0.1778(2)	0.4634(2)	0.52(2)/0.48(2)	0.0148(6)
Sr(2)	0.3380(4)	0.1416(2)	0.1977(2)	1	0.0148(6)
Sr(3)	0.5	0	0.5	1	0.0148(6)
Sr(4)	0.1629(4)	0.0126(2)	0.8364(2)	1	0.0148(6)
Mn(1)	0.5694(7)	0.1649(4)	0.9228(4)	1	0.0101(7)
Mn(2)	0.7709(6)	0.1772(3)	0.7220(4)	1	0.0101(7)
O(1)	0.5044(4)	0.1082(2)	0.7263(2)	1	0.0108(6)
O(2)	0.6734(5)	0.1726(2)	0.3349(3)	1	0.0108(6)
O(3)	0.8422(4)	0.0929(2)	0.9172(3)	1	0.0108(6)
O(4)	0.3377(4)	0.2462(2)	0.9570(2)	1	0.0140(6)
O(5)	0.8460(3)	0.0270(2)	0.6205(3)	1	0.0140(6)
O(6)	0.0083(4)	0.2686(2)	0.6990(2)	1	0.0140(6)
O(7)	0.5	0	0	1	0.019(1)

Space group: $P2_1/c$ $a = 6.904(4)$ Å, $b = 9.856(7)$ Å, $c = 10.165(7)$ Å, $\beta = 93.604(1)^\circ$ $\chi^2 = 2.06$, wRp = 5.82%, Rp = 4.83%.

Table 5
Refined structural parameters for $BaSr_6Mn_4O_{13}$

	x	*y*	*z*	Fraction	U_{iso}
Sr(1)	0.0067(3)	0.1824(2)	0.4636(2)	1	0.0146(6)
Sr(2)	0.3442(3)	0.1441(2)	0.2002(2)	1	0.0146(6)
Ba/Sr(3)	0.479(1)	0.9839(8)	0.4889(9)	0.074(8)/0.426(8)	0.0146(6)
Ba/Sr(4)	0.1627(4)	0.0107(2)	0.8364(2)	0.19(1)/0.81(1)	0.0146(6)
Mn(1)	0.5772(6)	0.1643(4)	0.9247(4)	1	0.0092(5)
Mn(2)	0.7623(6)	0.1677(4)	0.7207(4)	1	0.0092(5)
O(1)	0.5098(4)	0.1035(3)	0.7321(2)	1	0.0099(6)
O(2)	0.6786(5)	0.1755(2)	0.3355(3)	1	0.0099(6)
O(3)	0.8350(4)	0.0908(2)	0.9170(3)	1	0.0099(6)
O(4)	0.3382(4)	0.2439(2)	0.9590(2)	1	0.0162(6)
O(5)	0.8530(4)	0.0278(2)	0.6262(3)	1	0.0162(6)
O(6)	0.0102(4)	0.2637(3)	0.7042(3)	1	0.0162(6)
O(7)	0.5	0	0	1	0.0090(1)

Space group: $P2_1/c$ $a = 6.904(4)$ Å, $b = 9.856(7)$ Å, $c = 10.165(7)$ Å, $\beta = 93.604(1)^\circ$ $\chi^2 = 2.09$, wRp = 5.31%, Rp = 5.44%.

Table 6
Refined bond lengths and bond valence sums of $A_7Mn_4O_{13}$ phases

Cation	Anion	$Sr_6CaMn_4O_{13}$		$Sr_7Mn_4O_{13}$		$BaSr_6Mn_4O_{13}$	
		Bond (Å)	BVS	Bond (Å)	BVS	Bond (Å)	BVS
Mn(1)	O(1)	2.062(4)	+3.16	2.051(4)	+3.05	2.072(5)	+3.07
	O(2)	1.968(5)		1.973(5)		1.971(5)	
	O(3)	1.992(5)		1.984(4)		1.928(5)	
	O(4)	1.821(5)		1.858(4)		1.879(5)	
	O(7)	1.859(4)		1.880(4)		1.882(4)	
Mn(2)	O(1)	1.941(5)	+2.97	1.895(4)	+3.03	1.865(5)	+2.98
	O(2)	1.992(4)		1.941(4)		2.042(5)	
	O(3)	2.145(5)		2.133(4)		2.164(5)	
	O(5)	1.873(4)		1.860(4)		1.814(5)	
	O(6)	1.876(5)		1.951(4)		1.972(5)	
Sr(1)	O(2)	2.535(4)		2.569(4)		2.53(1)	
	O(3)	2.529(3)		2.556(3)		2.55(1)	
	O(4)	2.380(4)		2.376(3)		2.40(2)	
	O(5)	2.411(3)		2.469(3)		2.487(9)	
	O(5)	2.465(3)		2.554(3)		2.52(1)	
	O(6)	2.699(3)		2.686(3)		2.692(4)	
	O(6)	2.519(3)		2.559(3)		2.572(4)	
Sr(2)							
	O(1)	2.697(3)		2.714(2)		2.713(4)	
	O(1)	2.747(3)		2.748(2)		2.748(4)	
	O(2)	2.603(4)		2.605(4)		2.630(4)	
	O(3)	2.804(3)		2.810(3)		2.850(3)	
	O(4)	2.617(3)		2.645(3)		2.640(3)	
	O(4)	2.817(3)		2.819(3)		2.856(3)	
	O(5)	2.811(3)		2.797(3)		2.853(4)	
	O(6)	2.414(4)		2.434(3)		2.481(4)	
	O(7)	2.710(2)		2.749(2)		2.755(3)	
Sr(3)	O(1)	2.498(2)		2.524(2)		2.40(1)	
	O(1)	2.498(2)		2.524(2)		2.73(1)	
	O(2)	2.689(3)		2.774(3)		2.864(9)	
	O(2)	2.689(3)		2.774(3)		2.655(9)	
	O(4)	2.732(2)		2.756(2)		2.872(8)	
	O(4)	2.732(2)		2.756(2)		2.709(8)	
	O(5)	2.589(2)		2.584(2)		2.891(8)	
	O(5)	2.589(2)		2.584(2)		2.509(8)	
Sr(4)	O(1)	2.804(4)		2.829(3)		2.832(4)	
	O(2)	2.777(4)		2.779(3)		2.804(4)	
	O(3)	2.675(4)		2.701(3)		2.698(4)	
	O(3)	2.509(4)		2.504(4)		2.578(4)	
	O(4)	2.804(3)		2.822(3)		2.849(4)	
	O(5)	2.953(4)		2.968(3)		2.931(4)	
	O(6)	2.662(3)		2.648(2)		2.731(4)	
	O(6)	3.005(3)		3.034(3)		2.992(4)	
	O(7)	2.723(3)		2.756(3)		2.777(3)	

fractions of the two phases are detailed in Table 7 with a fit to the data shown in Fig. 4.

4. Discussion

The topotactic reduction of $A_7Mn_4O_{15}$ ($A_7 = Sr_7$, $BaSr_6$, Sr_6Ca) phases with CaH_2 at 300 °C rapidly yields the Mn(III) containing phases $A_7Mn_4O_{13}$. On reduction the manganese coordination number is lowered from 6 to 5 (Fig. 5). The resulting coordination environments around the two crystallographically distinct manganese sites are both significantly distorted. The Mn(1)–O(1) and Mn(2)–O(3) bond lengths are significantly longer than the remaining manganese oxygen bond lengths in the material. As shown in Fig. 5 these lengthened bonds are opposite the newly vacant O(8) anion sites and thus lie at the 'caps' of the MnO_5 square based pyramids. The total stoichiometry and the bond valence sums (BVS) [16] for both manganese sites are consistent with Mn(III) (BVS Mn(1) = +3.05, BVS Mn(2) = +3.03).

The selectivity of the oxide deintercalation reaction that converts $Sr_7Mn_4O_{15}$ into $Sr_7Mn_4O_{13}$ and $Sr_7Mn_4O_{12}$ is striking. Anions are removed exclusively from sites which link MnO_6 octahedra in an apex-shared manner (O(7) and O(8)). This is a direct contrast to the observed anion vacancy location preferences of the structurally similar 4H-$BaMnO_{2.66}$ and other $BaMnO_{3-x}$ phases [9,17]. In these reduced oxides the anion vacancies are located almost exclusively in face-shared anion sites. Given the strong structural similarity between 4H-$BaMnO_3$ and $Sr_7Mn_4O_{15}$ an explanation for their differing behaviour is required.

Table 7
Refined lattice parameters and phase fractions for $Sr_7Mn_4O_{14.05}$. The unrefined lattice parameters of $Sr_7Mn_4O_{15}$ phase included in the fit were obtained from Ref. [6]

a(Å)	b(Å)	c(Å)	β(°)	Fraction	Composition
6.8354(4)	9.6278(6)	10.2965(5)	92.886(6)	89(1)%	$Sr_7Mn_4O_{13.93(4)}$
6.8124	9.6152	10.3744	91.865	11(1)%	$Sr_7Mn_4O_{15}$

$\chi^2 = 1.36$, wRp = 7.54%, Rp = 6.43%.

Previous studies of topotactically reduced complex oxides have shown that the preferred location of anion vacancies within structures is influenced by the coordination preferences of all the cations in the phase [12]. Explicitly this means both the transition metal ions (*B*-cations) that are being reduced, and the "*A*-cations" which are not. If we consider the BVS of these ions it becomes clear that on reduction the BVS of the transition metal needs to decline. Conversely the BVS of the *A*-cations needs to be maintained. The new coordination requirements of the transition element can be met by lowering its coordination number and/or lengthening the average *B*-cation–anion bond length. However if anions are removed from the coordination environment of the *A*-cations, the average *A*-cation–anion bond length needs to decrease. The optimum coordination environments of both *A* and *B*-cations are best achieved on reduction by removing anions with strong (short) bonds to the *B*-cations and weak (long) bonds to the *A*-cations. Thus reducing the BVS of the *B*-cations with the smallest change to the BVS of the *A*-cations. So in the specific examples of $Sr_7Mn_4O_{15}$ and 4H-$BaMnO_3$ we would expect to remove oxide ions with short bonds to Mn and long bonds to Sr/Ba.

This idea can be evaluated for the $Sr_7Mn_4O_{15}$ structure by calculating the contribution each anion site makes to the BVS of the manganese and strontium cations as shown in Table 8. It should be noted that in this instance BVS are

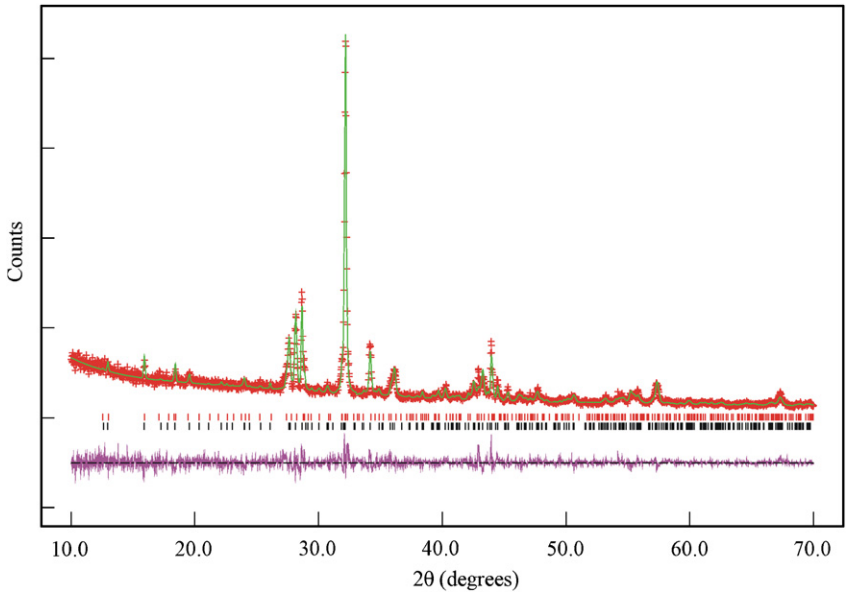

Fig. 4. Observed, calculated and difference plot from the two-phase refinement of $Sr_7Mn_4O_{14}$. Lower tick marks indicate peak positions of $Sr_7Mn_4O_{13.93(4)}$, upper tick marks $Sr_7Mn_4O_{15}$.

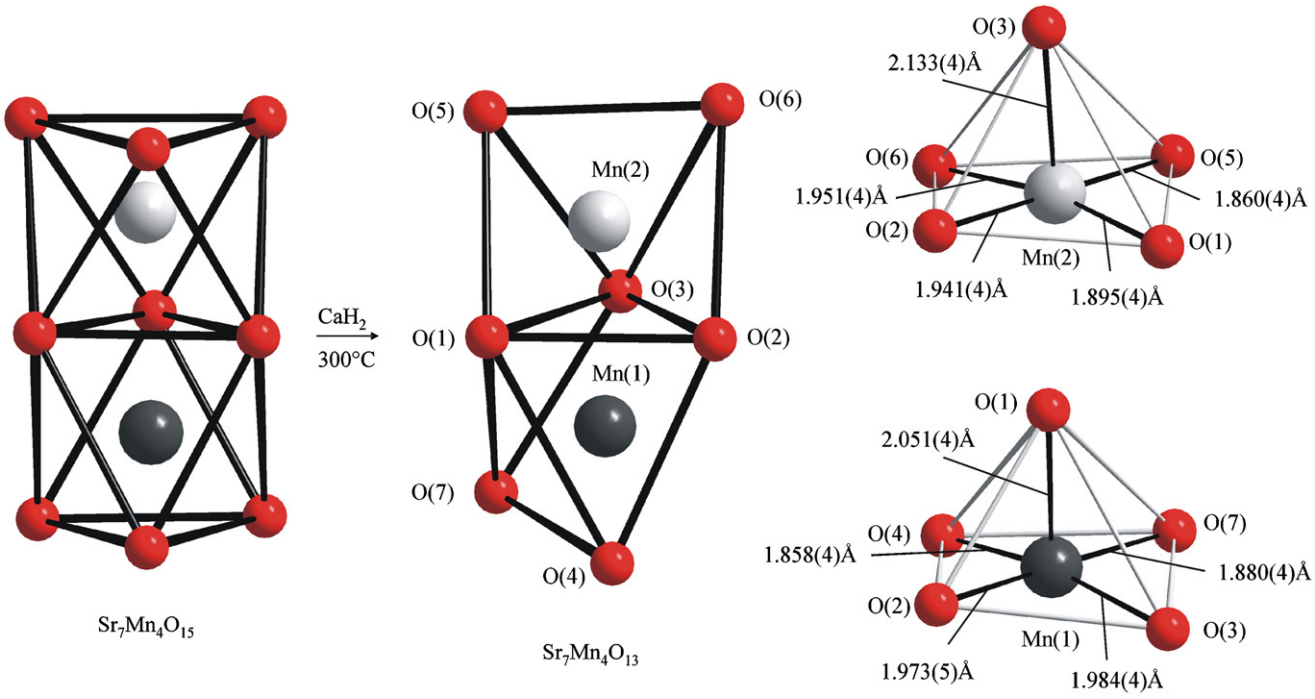

Fig. 5. The Manganese co-ordination spheres in $Sr_7Mn_4O_{13}$.

Table 8
Bond valence sums calculated for the anion sites in $Sr_7Mn_4O_{15}$ and $Sr_7Mn_4O_{13}$

	Face-shared			Non-bridging			Apex-shared	
$Sr_7Mn_4O_{15}$	O(1)	O(2)	O(3)	O(4)	O(5)	O(6)	O(7)	O(8)
Sr BVS	0.84	1.14	0.84	1.22	1.17	1.21	0.85	1.17
Mn BVS	1.15	1.15	1.26	0.54	0.77	0.79	1.52	1.56
Mn BVS-Sr BVS	+0.31	+0.01	+0.42	−0.68	−0.40	−0.42	+0.67	+0.39
$Sr_7Mn_4O_{13}$	O(1)	O(2)	O(3)	O(4)	O(5)	O(6)	O(7)	
Sr BVS	0.88	0.92	1.03	1.24	1.26	1.29	0.73	
Mn BVS	1.16	1.18	0.92	0.78	0.76	0.60	1.45	
Mn BVS-Sr BVS	+0.28	+0.26	−0.11	−0.46	−0.50	−0.69	+0.72	

not being used to calculate the 'valence' of the cation in the structure. They are being used to crudely compare the contribution each anion site makes to the lattice energy of the phase (although not calculating it explicitly) by taking into account not only the number and length of anion–cation contacts involved, but also the non-linear relation between bond-length and strength.

Even with the above caveats in mind, it is immediately clear from the data in Table 8 that anion sites O(4–6) stabilize the BVS of strontium more strongly than that of Mn (negative value for BVS_{Mn}-BVS_{Sr}). This is not surprising given that anions O(4–6) do not bridge between MnO_6 octahedra and so have five strontium ions and one manganese ion in their first coordination shell. Therefore these anions are not removed on reduction, as the resulting coordination spheres around the metal cations would be far from optimal. The remaining anion sites all have positive values for BVS_{Mn}–BVS_{Sr}. It can be seen that the apex-bridging sites (O(7) and O(8)) stabilize the BVS of manganese the most strongly leading to large positive values of BVS_{Mn}–BVS_{Sr}. Anion site O(3) has a similarly large value of BVS_{Mn}–BVS_{Sr}, however, Table 8 shows that on reduction the structure distorts to change the coordination environment around site O(3) to strengthen the interaction with strontium while weakening that with manganese to result in a negative BVS_{Mn}–BVS_{Sr} for the anion site in the $Sr_7Mn_4O_{13}$ structure. Therefore the removal of anions from sites O(8) and then O(7) (on further reduction from $Sr_7Mn_4O_{13}$ to $Sr_7Mn_4O_{12}$) is favoured as the structures produced on reduction maintain the coordination requirements of both the strontium and manganese cations.

A similar analysis of the structure of 4H-$BaMnO_3$ reveals a more positive value of BVS_{Mn}–BVS_{Ba} for the face-shared anion site in this phase, when compared with the apex-shared site, consistent with the observed anion vacancy locations in 4H-$BaMnO_{3-x}$ [9]. Thus the observed selectivity for removing the apex-bridging anions on reduction of $Sr_7Mn_4O_{15}$ is explained as a coincidence of the structural arrangement of the phase. The shorter bond lengths to manganese of anions which bridge MnO_6 octahedra in an apex-shared manner

rather than a face-shared manner combined with the disposition of the strontium cations lead to more optimal cation coordination polyhedra when apex-shared anions are removed. Similarly the particular structural arrangement of cations in 4H-$BaMnO_{2.66}$ and other $BaMnO_{3-x}$ phases favours the removal of face-shared ions as this best satisfies the coordination requirements of both the *A*- and *B*-cations in this structure.

Partial substitution of calcium and barium for strontium in $Sr_7Mn_4O_{15}$ follows the distribution reported by Vente et al. [10] with calcium residing on the small Sr(1) site and barium on the larger Sr(3) and Sr(4) sites (Tables 4 and 5). The *A*-cation substitutions have the expected influence on the *A*-cation coordination spheres but appear to have no effect on the anion vacancy distribution on reduction. Presumably this is because only small amounts of strontium can be replaced in this phase and these quantities are insufficient to change the energetics of anion vacant materials.

The magnetic characterisation of these phases will be reported elsewhere.

In conclusion it can be seen that the different anion vacancy distributions in reduced 'hexagonal' manganates can be rationalized by considering all the cations in the structure. This suggests a degree of structural predictability and/or control can be achieved in the vacancy ordering of such phases.

Acknowledgments

We thank R. M. Ibberson for assistance collecting neutron powder diffraction data and the Royal Society and EPSRC for funding this work.

Appendix A. Supplementary Materials

Supplementary data associated with this article can be found at online version doi:10.1016/j.jssc.2007.08.012

References

[1] K. Chahara, T. Ohno, M. Kasao, Y. Kozono, Appl. Phys. Lett. 63 (1993) 1990.
[2] P. Schiffer, A.P. Ramirez, W. Bao, S.-W. Cheong, Phys. Rev. Lett. 75 (1995) 3336.
[3] R. von Helmolt, J. Wecker, B. Holzapfel, L. Schultz, K. Sanwer, Phys. Rev. Lett. 71 (1993) 2331.
[4] J.F. Mitchell, J.E. Millburn, M. Medarde, D.N. Argyriou, J.D. Jorgensen, J. Appl. Phys. 85 (1999) 4352.
[5] K. Ruck, M. Sgraja, G. Krabbes, K. Door, K.-H. Muller, M. Khristov, J. Alloys Compds. 306 (2000) 151.
[6] J.F. Vente, K.V. Kamenev, D.A. Sokolov, Phys. Rev. B 64 (2001) 214403.
[7] T. Negas, R.S. Roth, J. Solid State Chem. 3 (1971) 323.
[8] M.A. Hayward, Chem. Commun. (2004) 170.
[9] J.J. Adkin, M.A. Hayward, J. Solid State Chem. 179 (2006) 70.
[10] J.F. Vente, J.R. Plaisier, D.J.W. Ijdo, K.V. Kamenev, Mater. Res. Bull. 35 (2000) 2437.
[11] M.A. Hayward, Chem. Mater. 17 (2005) 670.
[12] M.A. Hayward, Chem. Mater. 18 (2006) 321.
[13] N.N. Greenwood, A. Earnshaw, Chemistry of the Elements, Pergamon Press, Oxford, 1997.
[14] A.C. Larson, R.B. Von Dreele, General Structure Analysis System. 2000, Los Alamos National Laboratory Report LAUR 86–748.
[15] L.J. Gillie, A.J. Wright, J. Hadermann, G. Van Tendeloo, C. Greaves, J. Solid State Chem. 167 (2002) 145.
[16] N.E. Brese, M. O'Keefe, Acta Crystallogr. Sect. B: Struct. Sci. B 47 (1991) 192–197.
[17] J.J. Adkin, M.A. Hayward, Chem. Mater. 19 (2007) 755.